

Model independent analysis of top quark forward-backward asymmetry at the Tevatron up to $\mathcal{O}(\alpha_s^2/\Lambda^2)$

Ding Yu Shao,¹ Chong Sheng Li,^{1,2,*} Jian Wang,¹

Jun Gao,¹ Hao Zhang,¹ and Hua Xing Zhu¹

¹*Department of Physics and State Key Laboratory of Nuclear Physics and Technology,
Peking University, Beijing 100871, China*

²*Center for High Energy Physics, Peking University, Beijing 100871, China*

Abstract

We present the complete calculations of the forward-backward asymmetry (A_{FB}) and the total cross section of top quark pair production induced by dimension-six four quark operators at the Tevatron up to $\mathcal{O}(\alpha_s^2/\Lambda^2)$. Our results show that next-to-leading order (NLO) QCD corrections can change A_{FB} and the total cross section by about 10%. Moreover, NLO QCD corrections reduce the dependence of A_{FB} and total cross section on the renormalization and factorization scales significantly. We also evaluate the total cross section and the charge asymmetry (A_{C}) induced by these operators at the Large Hadron Collider (LHC) up to $\mathcal{O}(\alpha_s^2/\Lambda^2)$, for the parameter space allowed by the Tevatron data. We find that the value of A_{C} induced by these operators is much larger than SM prediction, and LHC has potential to discover these NP effects when the measurement precision increases.

PACS numbers: 14.65.Ha, 12.38.Bx, 12.60.-i

*Electronic address: csli@pku.edu.cn

I. INTRODUCTION

The top quark is the heaviest particle discovered so far, with a mass close to the electroweak symmetry breaking scale. Thus it is a wonderful probe for the electroweak breaking mechanism and new physics (NP) beyond the standard model (SM) through its productions and decays at colliders. The forward-backward asymmetry (A_{FB}) of the top quark pair production is one of the interesting observables at hadron colliders. Within the SM, A_{FB} is absent at the tree level in QCD due to charge symmetry, and occurs at next-to-leading order (NLO) $\mathcal{O}(\alpha_s^3)$ in QCD with the prediction $A_{\text{FB}} \sim 6\%$ in the $t\bar{t}$ rest frame [1–6]. In the last few years, DØ and CDF Collaborations measured A_{FB} at the Tevatron [7–10]. Recently, the CDF Collaborations announced that, for the invariant mass of the top quark pair $m_{t\bar{t}} \geq 450$ GeV, the measured asymmetry, $A_{\text{FB}} = 0.475 \pm 0.114$ [9], differs by 3.4σ from the SM predictions $A_{\text{FB}} = 0.088 \pm 0.013$, which has aroused many discussions of explaining this deviation in NP model, including new gauge bosons, axigluons and so on[11–68].

Since we do not know which type of NP will be responsible for this deviation, it is interesting to study the A_{FB} in a model independent way, using an effective Lagrangian. In general, NP scale relevant to A_{FB} is large enough so that the heavy fields have been integrated out at the low energy scale. At the Tevatron, the subprocess $q\bar{q} \rightarrow t\bar{t}$ dominates over top quark pair production, so only contributions from dimension-six four quark operators to the $t\bar{t}$ production are considered. Similar approach had been adopted for the dijet production to constrain the composite scale of light quarks [69–73]. The relevant effective Lagrangian can be written as

$$\mathcal{L}_{NP} = \frac{1}{\Lambda^2} \sum_{A,B} [C_{AB}^1 (\bar{q}_A \gamma_\mu q_A) (\bar{t}_B \gamma^\mu t_B) + C_{AB}^8 (\bar{q}_A T^a \gamma_\mu q_A) (\bar{t}_B T^a \gamma^\mu t_B)], \quad (1)$$

where $\{A, B\} = \{L, R\}$ with $q = (u, d)^T, (c, s)^T$. Up to $\mathcal{O}(\alpha_s/\Lambda^2)$, the NP contributions to the total cross section and the A_{FB} are clear in the vector-axial basis [28, 38, 74], as compared with the chirality basis. Only the axial-axial current combination contributions to the A_{FB} , and the vector-vector operator contributes to the total cross section. However, this is no longer true up to $\mathcal{O}(\alpha_s^2/\Lambda^2)$. The chirality basis is the preferred one when studying the chiral structure of NP effects much above the Electroweak scale, so we choose to work in the chirality basis. The contributions to A_{FB} at leading order (LO) from such operators has been explored in Refs. [19, 28, 29, 31, 45, 75]. It is shown that the A_{FB} observed at the Tevatron

can be explained by above operators for suitable parameters. As we know, the LO cross section at hadron colliders suffers from large uncertainties due to the arbitrary choice of the renormalization scale and factorization scale, thus it is important to include NLO corrections to improve theoretical predictions. Besides, at the NLO level, virtual corrections, real gluon emission and massless (anti)quark emission can lead to a sizeable difference between the differential top and anti-top production process [1, 2], which will contribute to A_{FB} .

In this paper, we present the complete NLO QCD calculations of A_{FB} and the total cross section of top quark pair production at the Tevatron induced by above operators, and we also study the top quark pair production at the Large Hadron Collider (LHC) induced by these operators at the NLO QCD level. Last year, LHC reported their first observation of top quark pair production, and will soon become a major top quark factory. At the LHC, the top quark pairs can be produced through quark antiquark annihilation $q\bar{q} \rightarrow t\bar{t}$ and gluon fusion $gg \rightarrow t\bar{t}$. Since gluon fusion channel dominates at the LHC, it is difficult to probe these four quark effective operators from early LHC results. However, it is still possible to detect these effects from above effective operators on the Charge Asymmetry (A_C) at the LHC, in the parameter space allowed by the Tevatron data, when the measurement precision increases.

The arrangement of this paper is as follows. In Sec. II we show the LO results. In Sec. III, we present the details of the NLO calculations, including the virtual and real corrections to the top quark pair production. Section IV contains the numerical results, and Section V is a brief summary.

II. LO RESULTS

Throughout our calculation, we adopt the same conventions as in Ref. [76] (see Sec. III A), and present the helicity amplitudes for $q\bar{q} \rightarrow t\bar{t}$ in the Four-Dimensional Helicity (FDH) regularization scheme [77]. The $t\bar{t}$ production amplitudes, including NP contributions, can be written as

$$\mathcal{M}_{t\bar{t}} = \alpha_s f_{\text{LO}}^{\text{SM}} + \frac{1}{\Lambda^2} f_{\text{LO}}^{\text{NP}} + \alpha_s^2 f_{\text{NLO}}^{\text{SM}} + \frac{\alpha_s}{\Lambda^2} f_{\text{NLO}}^{\text{NP}} + \dots, \quad (2)$$

and thus the partonic cross section, up to $\mathcal{O}(\alpha_s^2/\Lambda^2)$, can be written as

$$\begin{aligned} \hat{\sigma}_{t\bar{t}} = & \alpha_s^2 f_{\text{LO}}^{\text{SM}} f_{\text{LO}}^{\text{SM}*} + 2 \frac{\alpha_s}{\Lambda^2} \mathcal{R}e (f_{\text{LO}}^{\text{SM}} f_{\text{LO}}^{\text{NP}*}) \\ & + 2\alpha_s^3 \mathcal{R}e (f_{\text{LO}}^{\text{SM}} f_{\text{NLO}}^{\text{SM}*}) + 2 \frac{\alpha_s^2}{\Lambda^2} [\mathcal{R}e (f_{\text{LO}}^{\text{NP}} f_{\text{NLO}}^{\text{SM}*}) + \mathcal{R}e (f_{\text{LO}}^{\text{SM}} f_{\text{NLO}}^{\text{NP}*})]. \end{aligned} \quad (3)$$

The LO Feynman diagrams for the subprocess $q(p_1)\bar{q}(p_2) \rightarrow t(p_3)\bar{t}(p_4)$ induced by the SM

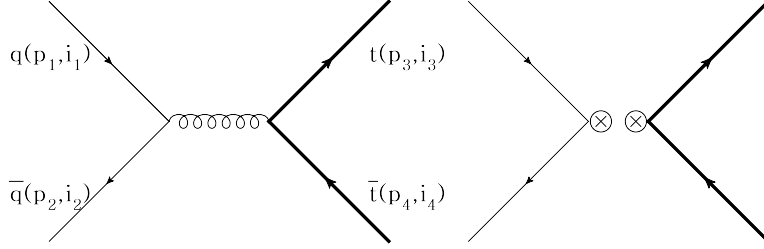


FIG. 1: LO Feynman diagrams for $q\bar{q} \rightarrow t\bar{t}$ induced by SM QCD and NP interactions.

QCD and the NP interactions are shown in Fig. 1, and their $(+ - ++)$ helicity amplitudes are

$$\mathcal{M}_{\text{LO}}^{\text{SM}}(+ - ++) = \frac{i8\pi\alpha_s m_t}{s} (\mathcal{M}_1 + \mathcal{M}_2) \mathcal{C}_8, \quad (4)$$

$$\mathcal{M}_{\text{LO}}^{\text{NP}}(+ - ++) = \frac{i2m_t}{\Lambda^2} [(\mathcal{M}_1 C_{\text{RR}}^1 + \mathcal{M}_2 C_{\text{RL}}^1) \mathcal{C}_1 + (\mathcal{M}_1 C_{\text{RR}}^8 + \mathcal{M}_2 C_{\text{RL}}^8) \mathcal{C}_8], \quad (5)$$

where the SM QCD and NP contributions are denoted by superscripts SM and NP, and Mandelstam variables s , t and u are defined as follows:

$$s = (p_1 + p_2)^2, \quad t = (p_1 - p_3)^2, \quad u = (p_1 - p_4)^2. \quad (6)$$

We define the following abbreviations for the color structures and matrix elements,

$$\begin{aligned} \mathcal{M}_1 &= \frac{\langle \eta_4 1 \rangle \langle \eta_3 | \mathbf{3} | 2 \rangle}{\langle 3^b \eta_3 \rangle \langle \eta_4 4^b \rangle}, & \mathcal{M}_2 &= \frac{\langle \eta_3 1 \rangle \langle \eta_4 | \mathbf{4} | 2 \rangle}{\langle 3^b \eta_3 \rangle \langle \eta_4 4^b \rangle}, \\ \mathcal{M}_3 &= \frac{\langle \eta_4 2 \rangle \langle \eta_3 | \mathbf{3} | 1 \rangle}{\langle 3^b \eta_3 \rangle \langle \eta_4 4^b \rangle}, & \mathcal{M}_4 &= \frac{\langle \eta_3 2 \rangle \langle \eta_4 | \mathbf{4} | 1 \rangle}{\langle 3^b \eta_3 \rangle \langle \eta_4 4^b \rangle}, \\ \mathcal{C}_1 &= \delta_{i_2 i_1} \delta_{i_3 i_4}, & \mathcal{C}_8 &= T_{i_2 i_1}^a T_{i_3 i_4}^a, \end{aligned} \quad (7)$$

where $i_{1\dots 4}$ are the color indices of the external quarks and the boldface momenta denotes massive vectors. We use the modified spinor helicity method suited for massive particles [78] in our calculations, and a recent application of this method can be found in the Ref [79].

The $(-+++)$ amplitudes are given by

$$\mathcal{M}_{\text{LO}}^{\text{SM}}(-+++)=\frac{i8\pi\alpha_s m_t}{s}(\mathcal{M}_3+\mathcal{M}_4)\mathcal{C}_8, \quad (8)$$

$$\mathcal{M}_{\text{LO}}^{\text{NP}}(-+++)=\frac{i2m_t}{\Lambda^2}[(\mathcal{M}_3C_{\text{LR}}^1+\mathcal{M}_4C_{\text{LL}}^1)\mathcal{C}_1+(\mathcal{M}_3C_{\text{LR}}^8+\mathcal{M}_4C_{\text{LL}}^8)\mathcal{C}_8]. \quad (9)$$

The amplitudes with other helicity configurations can be obtained from $(+-++)$ and $(-+++)$ by exchanging light-like momenta p^b and η [76, 79]. At the LO, there is only vector current coupling $\bar{\psi}\gamma^\mu\psi$ at the massive quark vertex. At the NLO, however, magnetic-momentum coupling $\bar{\psi}(i\sigma^{\mu\nu}(p_3+p_4)_\mu)\psi/(2m_t)$ is induced from loop diagrams. For completeness we list the matrix elements for magnetic-moment interaction,

$$\begin{aligned} \mathcal{M}_1^{(m)} &= \frac{m_t^2\langle\eta_31\rangle\langle\eta_41\rangle[21]}{\langle 3^b\eta_3\rangle\langle\eta_44^b\rangle}, & \mathcal{M}_2^{(m)} &= \frac{\langle 12\rangle\langle\eta_3\mathbf{3}2\rangle\langle\eta_4\mathbf{4}2\rangle}{\langle 3^b\eta_3\rangle\langle\eta_44^b\rangle}, \\ \mathcal{M}_3^{(m)} &= \frac{m_t^2\langle\eta_32\rangle\langle\eta_42\rangle[21]}{\langle 3^b\eta_3\rangle\langle\eta_44^b\rangle}, & \mathcal{M}_4^{(m)} &= \frac{\langle 12\rangle\langle\eta_3\mathbf{3}1\rangle\langle\eta_4\mathbf{4}1\rangle}{\langle 3^b\eta_3\rangle\langle\eta_44^b\rangle}. \end{aligned} \quad (10)$$

After phase space integration, the $\mathcal{O}(\alpha_s/\Lambda^2)$ partonic differential cross section is

$$\frac{d\hat{\sigma}_{\text{LO}}^{\text{NP}}}{d\cos\theta}=\frac{\beta}{18}\frac{\alpha_s}{\Lambda^2}\left[\frac{1}{4}(1+\rho+\beta^2\cos^2\theta)(C_{\text{LR}}^8+C_{\text{RR}}^8)+\frac{1}{2}\beta\cos\theta(C_{\text{RR}}^8-C_{\text{LR}}^8)\right], \quad (11)$$

where $\rho=4m_t^2/s$, $\beta=\sqrt{1-\rho^2}$, and θ is the polar angle between the incoming quark and the outgoing top quark in the $t\bar{t}$ rest frame. The color and spin indices are averaged(summed) over initial(final) states. In Eq. (11) the term linear in $\cos\theta$ could generate A_{FB} proportional to $(C_{\text{RR}}^8-C_{\text{LR}}^8)$ and the rest terms contribute to the total cross section proportional to $(C_{\text{RR}}^8+C_{\text{LR}}^8)$. These relations will be changed at the NLO level.

The LO total cross section at the hadron collider is obtained by convoluting the partonic level cross section with the Parton Distribution Function (PDF) $f_{i/A}$ for the initial hadron A:

$$\sigma_{\text{LO}}=\sum_{a,b}\int_\tau^1 dx_a\int_{\tau/x_a}^1 dx_b f_{a/A}(x_a,\mu_f)f_{b/B}(x_b,\mu_f)\hat{\sigma}_{\text{LO}}, \quad (12)$$

where $\tau=4m_t^2/s$. The sum is over all possible initial partons.

III. NLO QCD CORRECTIONS

The NLO corrections to the top pair production consist of the virtual corrections, generated by loop diagrams of colored particles, and the real corrections with the radiation of

a real gluon or a massless (anti)quark. We carried out all the calculations in the 't Hooft-Feynman gauge and used the FDH scheme to regularize all the divergences. Moreover, for the real corrections, we used the dipole subtraction method with massive partons [80] to separate the infrared (IR) divergences, which is convenient for the case of massive Feynman diagrams and provides better numerical accuracy.

A. Virtual corrections

The virtual corrections for the top quark pair production include the box diagrams, triangle diagrams, and self-energy diagrams in SM QCD and NP as shown in Fig. 2 and Fig. 3. We have calculated the one-loop helicity amplitudes for the SM process, and find complete agreement with those in the Ref. [76, 81]. Here we only list the NP contributions.

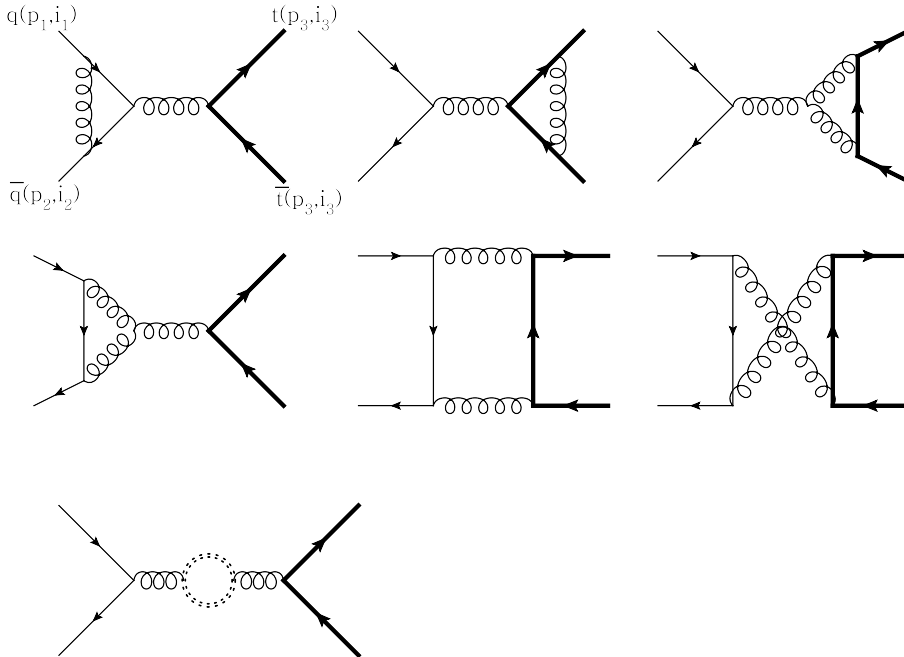


FIG. 2: One-loop virtual Feynman diagrams for $q\bar{q} \rightarrow t\bar{t}$ induced by SM QCD interactions.

All the ultraviolet (UV) divergences in the loop diagrams are canceled by counterterms for the wave functions of the external fields ($\delta Z_q, \delta Z_t$), and the Wilson coefficients $\delta Z_{C_{AB}^i}$. For the external fields, we fix all the renormalization constants using on-shell subtraction,

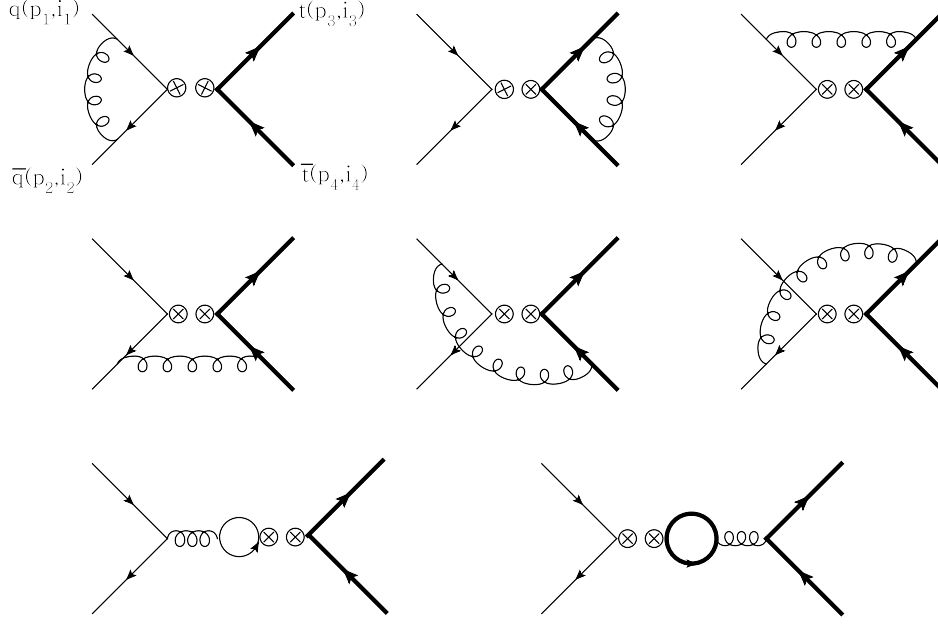


FIG. 3: One-loop virtual Feynman diagrams for $q\bar{q} \rightarrow t\bar{t}$ induced by NP interactions.

and, therefore, they also have IR singularities

$$\delta Z_q = -\frac{\alpha_s}{4\pi} C_\varepsilon C_F \left(\frac{1}{\varepsilon_{UV}} - \frac{1}{\varepsilon_{IR}} \right), \quad (13)$$

$$\delta Z_t = -\frac{\alpha_s}{4\pi} C_\varepsilon C_F \left(\frac{1}{\varepsilon_{UV}} + \frac{2}{\varepsilon_{IR}} + 5 - 3 \ln \frac{m_t^2}{\mu_r^2} \right), \quad (14)$$

where $C_\varepsilon = (4\pi)^\varepsilon \frac{1}{\Gamma(1-\varepsilon)}$, $C_F = 4/3$ and μ_r is the renormalization scale. For counterterms of the Wilson coefficients $\delta Z_{C_{AB}^i}$, we adopted the $\overline{\text{MS}}$ scheme

$$\delta Z_{C_{AB}^i} = \frac{\alpha_s}{4\pi} C_\varepsilon C_F \frac{1}{\varepsilon_{UV}} \begin{pmatrix} 0 & \frac{9}{8} & 0 & 0 & 0 & 0 & 0 & 0 \\ \frac{1}{4} & \frac{n_f-5}{16} & 0 & \frac{1}{16} & 0 & \frac{n_f}{16} & 0 & 0 \\ 0 & 0 & 0 & -\frac{9}{8} & 0 & 0 & 0 & 0 \\ 0 & \frac{1}{16} & -\frac{1}{4} & \frac{n_f-20}{16} & 0 & 0 & 0 & \frac{n_f}{16} \\ 0 & 0 & 0 & 0 & 0 & -\frac{9}{8} & 0 & 0 \\ 0 & \frac{n_f}{16} & 0 & 0 & -\frac{1}{4} & \frac{n_f-20}{16} & 0 & \frac{1}{16} \\ 0 & 0 & 0 & 0 & 0 & 0 & 0 & \frac{9}{8} \\ 0 & 0 & 0 & \frac{n_f}{16} & 0 & \frac{1}{16} & \frac{1}{4} & \frac{n_f-5}{16} \end{pmatrix}, \quad (15)$$

where $n_f = 5$ is the number of massless quarks appearing in the closed loop diagram, and the order of the Wilson coefficients is

$$(C_{LL}^1, C_{LL}^8, C_{LR}^1, C_{LR}^8, C_{RL}^1, C_{RL}^8, C_{RR}^1, C_{RR}^8). \quad (16)$$

We have considered mixing effects of different color and chiral operators, and the evolution equations of the Wilson coefficients are given in the Appendix B. The renormalized virtual amplitudes can be written as

$$\mathcal{M}^V = \mathcal{M}^{\text{unren}} + \mathcal{M}^{\text{con}}. \quad (17)$$

Here $\mathcal{M}^{\text{unren}}$ contains the self-energy and vertex corrections, and \mathcal{M}^{con} are the corresponding counterterms. The renormalized amplitude \mathcal{M}^V is UV finite, but still contains IR divergences, which are given by

$$\mathcal{M}_{\text{SM}}^{\text{IR}} = \frac{\alpha_s}{2\pi} C_\varepsilon C_F [f_{\text{os}}^{\text{IR}} \mathcal{C}_1 \mathcal{M}_8^{\text{SM}} + f_{\text{oo}}^{\text{IR}} \mathcal{C}_8 \mathcal{M}_8^{\text{SM}}], \quad (18)$$

$$\mathcal{M}_{\text{NP}}^{\text{IR}} = \frac{\alpha_s}{2\pi} C_\varepsilon C_F [f_{\text{ss}}^{\text{IR}} \mathcal{C}_1 \mathcal{M}_1^{\text{NP}} + f_{\text{so}}^{\text{IR}} \mathcal{C}_8 \mathcal{M}_1^{\text{NP}} + f_{\text{os}}^{\text{IR}} \mathcal{C}_1 \mathcal{M}_8^{\text{NP}} + f_{\text{oo}}^{\text{IR}} \mathcal{C}_8 \mathcal{M}_8^{\text{NP}}], \quad (19)$$

where we define the IR divergence coefficients $f_{\text{ss}}^{\text{IR}}$, $f_{\text{so}}^{\text{IR}}$, $f_{\text{os}}^{\text{IR}}$ and $f_{\text{oo}}^{\text{IR}}$ for different color configurations, "s" for singlet and "o" for octet,

$$f_{\text{ss}}^{\text{IR}} = -\frac{1}{\varepsilon_{\text{IR}}^2} + \frac{1}{\varepsilon_{\text{IR}}} \left[\frac{1}{2} \left(\beta + \frac{1}{\beta} \right) \ln \left(\frac{\beta+1}{\beta-1} \right) + \ln \left(\frac{-s}{\mu_r^2} \right) - \frac{5}{2} \right], \quad (20)$$

$$f_{\text{so}}^{\text{IR}} = \frac{3}{2} \ln \left(\frac{t_1}{u_1} \right) \frac{1}{\varepsilon_{\text{IR}}}, \quad (21)$$

$$f_{\text{os}}^{\text{IR}} = \frac{1}{3} \ln \left(\frac{t_1}{u_1} \right) \frac{1}{\varepsilon_{\text{IR}}}, \quad (22)$$

$$f_{\text{oo}}^{\text{IR}} = -\frac{1}{\varepsilon_{\text{IR}}^2} + \frac{1}{\varepsilon_{\text{IR}}} \left[-\frac{1}{16} \left(\beta + \frac{1}{\beta} \right) \ln \left(\frac{\beta+1}{\beta-1} \right) - \frac{9}{8} \ln \left(\frac{m_t^2}{\mu_r^2} \right) - \frac{1}{8} \ln \left(\frac{-s}{\mu_r^2} \right) + \frac{7}{4} \ln \left(\frac{t_1}{\mu_r^2} \right) + \frac{1}{2} \ln \left(\frac{u_1}{\mu_r^2} \right) - \frac{5}{2} \right], \quad (23)$$

where $t_1 = m_t^2 - t$, $u_1 = m_t^2 - u$ and $\mathcal{M}_1^{\text{NP}}$, $\mathcal{M}_8^{\text{NP}}$ and $\mathcal{M}_8^{\text{SM}}$ are defined as follows,

$$\mathcal{M}_{\text{LO}}^{\text{SM}} = \mathcal{M}_8^{\text{SM}} \mathcal{C}_8, \quad (24)$$

$$\mathcal{M}_{\text{LO}}^{\text{NP}} = \mathcal{M}_1^{\text{NP}} \mathcal{C}_1 + \mathcal{M}_8^{\text{NP}} \mathcal{C}_8. \quad (25)$$

Since we only consider high order corrections up to $\mathcal{O}(\alpha_s^2/\Lambda^2)$, the IR divergences of the virtual corrections can be written as

$$\begin{aligned} & 2\mathcal{R}e [\mathcal{M}_{\text{SM}}^{\text{IR}} \mathcal{M}_{\text{NP}}^{\text{LO}*}] + 2\mathcal{R}e [\mathcal{M}_{\text{NP}}^{\text{IR}} \mathcal{M}_{\text{SM}}^{\text{LO}*}] \\ &= \frac{\alpha_s}{\pi} C_\varepsilon C_F [(9f_{\text{os}}^{\text{IR}} + 2f_{\text{so}}^{\text{IR}}) \mathcal{R}e (\mathcal{M}_1^{\text{NP}*} \mathcal{M}_8^{\text{SM}}) + 4f_{\text{oo}}^{\text{IR}} \mathcal{R}e (\mathcal{M}_8^{\text{NP}*} \mathcal{M}_8^{\text{SM}})]. \end{aligned} \quad (26)$$

The finite terms in $\mathcal{M}_{\text{NP}}^V$ are given in the Appendix A.

B. Real corrections

At the NLO level the real corrections consist of the radiations of an additional gluon or massless (anti)quark in the final states, including the subprocess

$$q\bar{q} \rightarrow t\bar{t}g, \quad gq(\bar{q}) \rightarrow t\bar{t}q(\bar{q}) \quad (27)$$

as shown in Fig.4 and Fig.5.

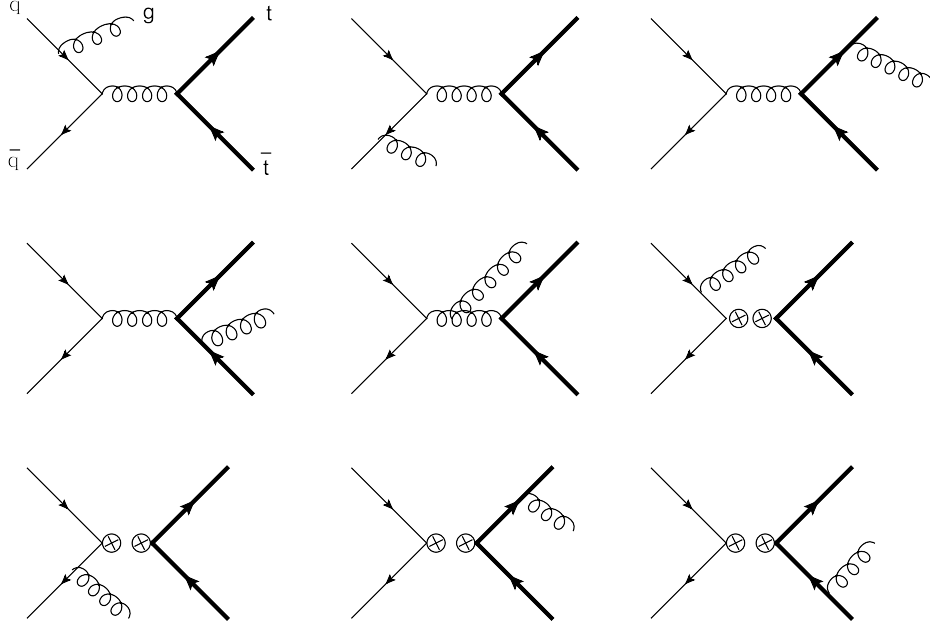


FIG. 4: Feynman diagrams for the real gluon emission contributions induced by SM QCD and NP interactions.

Before performing the numerical calculations, we need to extract the IR divergences in the real corrections. In the dipole formalism this is done by subtracting some dipole terms from the real corrections to cancel the singularities and large logarithms exactly, and then the real corrections become integrable in four dimensions. On the other hand, these dipole subtraction terms are analytically integrable in n dimensions over one-parton subspaces, which give ε poles that represent the soft and collinear divergences. Then we can add them to the virtual corrections to cancel the ε poles, and ensure the virtual corrections are also integrable in four dimensions. This whole procedure can be illustrated by the formula [80]:

$$\hat{\sigma}^{\text{NLO}} = \int_{m+1} [(d\hat{\sigma}^{\text{R}})_{\varepsilon=0} - (d\hat{\sigma}^{\text{A}})_{\varepsilon=0}] + \int_m \left[d\hat{\sigma}^{\text{V}} + \int_1 d\hat{\sigma}^{\text{A}} \right]_{\varepsilon=0}, \quad (28)$$

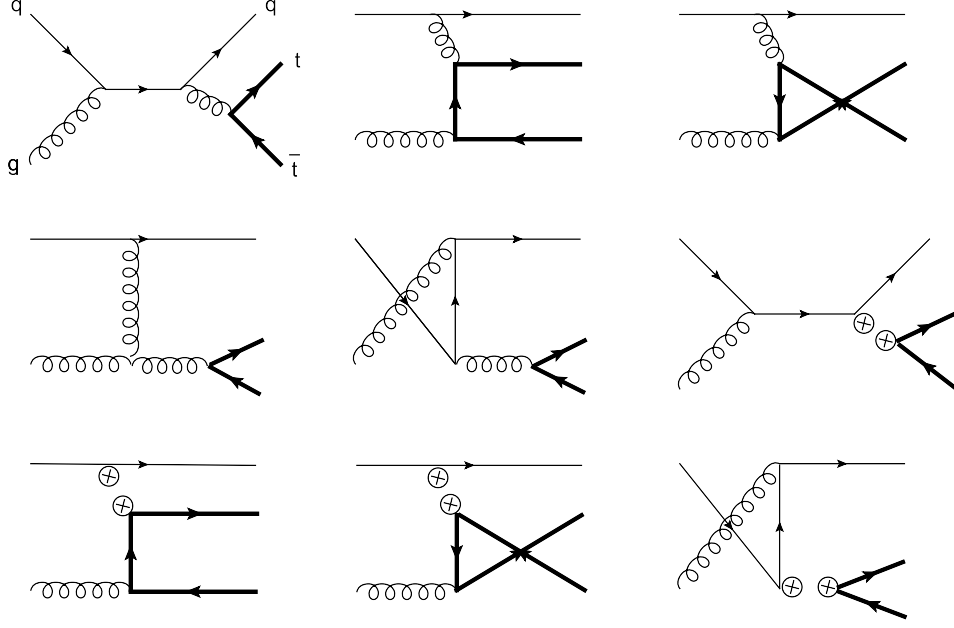


FIG. 5: Feynman diagrams for the massless quark emission contributions induced by SM QCD and NP interactions.

where m is the number of final state particles at the LO, and $d\hat{\sigma}^A$ is a sum of the dipole terms. Besides, at hadron colliders, we have to include the well-known collinear subtraction counterterms in order to cancel the collinear divergences arising from the splitting processes of the initial state massless partons. Here we use the $\overline{\text{MS}}$ scheme and the corresponding NLO PDFs.

For the process with two initial state hadrons, the dipole terms can be classified into four groups, the final-state emitter and final-state spectator type,

$$\mathcal{D}_{ij,k}(p_1, \dots, p_{m+1}) = -\frac{1}{(p_i + p_j)^2 - m_{ij}^2} m \langle \dots, \tilde{i}j, \dots, \tilde{k}, \dots | \frac{\mathbf{T}_k \cdot \mathbf{T}_{ij}}{\mathbf{T}_{ij}^2} \mathbf{V}_{ij,k} | \dots, \tilde{i}j, \dots, \tilde{k}, \dots \rangle_m, \quad (29)$$

the final-state emitter and initial-state spectator type,

$$\mathcal{D}_{ij}^a(p_1, \dots, p_{m+1}; p_a, \dots) = -\frac{1}{(p_i + p_j)^2 - m_{ij}^2} \frac{1}{x_{ij,a}} m_{,a} \langle \dots, \tilde{i}j, \dots; \tilde{a}, \dots | \frac{\mathbf{T}_a \cdot \mathbf{T}_{ij}}{\mathbf{T}_{ij}^2} \mathbf{V}_{ij}^a | \dots, \tilde{i}j, \dots; \tilde{a}, \dots \rangle_{m,a}, \quad (30)$$

the initial-state emitter and final-state spectator type,

$$\mathcal{D}_j^{ai}(p_1, \dots, p_{m+1}; p_a, \dots) = -\frac{1}{2p_a p_i} \frac{1}{x_{ij,a}} m_{,\tilde{a}i} \langle \dots, \tilde{j}, \dots; \tilde{a}i, \dots | \frac{\mathbf{T}_j \cdot \mathbf{T}_{ai}}{\mathbf{T}_{ai}^2} \mathbf{V}_j^{ai} | \dots, \tilde{j}, \dots; \tilde{a}i, \dots \rangle_{m,\tilde{a}i}, \quad (31)$$

and the initial-state emitter and initial-state spectator type,

$$\begin{aligned} \mathcal{D}^{ai,b}(p_1, \dots, p_{m+1}; p_a, p_b) = \\ -\frac{1}{2p_a p_i} \frac{1}{x_{i,ab}} \langle \dots; \tilde{a}i, b | \frac{\mathbf{T}_b \cdot \mathbf{T}_{ai}}{\mathbf{T}_{ai}^2} \mathbf{V}^{ai,b} | \dots; \tilde{a}i, b \rangle_{m, \tilde{a}i}, \end{aligned} \quad (32)$$

where a, b and i, j, \dots are the initial and final state partons, and \mathbf{T} and \mathbf{V} are the color charge operators and dipole functions acting on the LO amplitudes, respectively. The explicit expressions for $x_{i,ab}$, $x_{ij,a}$ and \mathbf{V} can be found in Ref. [80]. The integrated dipole functions together with the collinear counterterms can be written in the following factorized form

$$\begin{aligned} \sim & \int d\Phi^{(m)}(p_a, p_b) \langle \dots; p_a, p_b | \mathbf{I}_{m+a+b}(\varepsilon) | \dots; p_a, p_b \rangle_{m,ab} \\ & + \sum_{a'} \int_0^1 dx \int d\Phi^{(m)}(xp_a, p_b) \langle \dots; xp_a, p_b | \mathbf{P}_{m+b}^{a,a'}(x) + \mathbf{K}_{m+b}^{a,a'}(x) | \dots; xp_a, p_b \rangle_{m,a'b} \\ & + (a \leftrightarrow b), \end{aligned} \quad (33)$$

where x is the momentum fraction of the splitting parton, $d\Phi^{(m)}$ contains all the factors apart from the squared amplitudes, \mathbf{I} , \mathbf{P} , and \mathbf{K} are insertion operators defined in [80]. For simplicity, in all the above formulas we do not show the jet functions that define the observables and are included in our numerical calculations.

The operators \mathbf{P} and \mathbf{K} provide finite contributions to the NLO corrections, and only the operator \mathbf{I} contains the IR divergences

$$\begin{aligned} \mathbf{I}|_{\text{IR}} = & -\frac{\alpha_s}{2\pi} \frac{(4\pi)^\varepsilon}{\Gamma(1-\varepsilon)} \left\{ \sum_j \sum_{k \neq j} \mathbf{T}_j \cdot \mathbf{T}_k \left[\left(\frac{\mu_r^2}{s_{jk}} \right)^\varepsilon \mathcal{V}(s_{jk}, m_j, m_k; \varepsilon_{\text{IR}}) + \frac{1}{\mathbf{T}_j^2} \Gamma_j(m_j, \varepsilon_{\text{IR}}) \right] \right. \\ & + \sum_j \mathbf{T}_j \cdot \mathbf{T}_a \left[2 \left(\frac{\mu_r^2}{s_{ja}} \right)^\varepsilon \mathcal{V}(s_{ja}, m_j, 0; \varepsilon_{\text{IR}}) + \frac{1}{\mathbf{T}_j^2} \Gamma_j(m_j, \varepsilon_{\text{IR}}) + \frac{1}{\mathbf{T}_a^2} \frac{\gamma_a}{\varepsilon_{\text{IR}}} \right] \\ & \left. + \mathbf{T}_a \cdot \mathbf{T}_b \left[\left(\frac{\mu_r^2}{s_{ab}} \right)^\varepsilon \left(\frac{1}{\varepsilon_{\text{IR}}^2} + \frac{1}{\mathbf{T}_a^2} \frac{\gamma_a}{\varepsilon_{\text{IR}}} \right) \right] + (a \leftrightarrow b) \right\}, \end{aligned} \quad (34)$$

with

$$\begin{aligned} \mathcal{V}(s_{jk}, m_j, m_k; \varepsilon_{\text{IR}}) &= \frac{1}{v_{jk}} \left(\frac{Q_{jk}^2}{s_{jk}} \right)^\varepsilon \times \left(1 - \frac{1}{2} \rho_j^{-2\varepsilon} - \frac{1}{2} \rho_k^{-2\varepsilon} \right) \frac{1}{\varepsilon_{\text{IR}}^2}, \\ \Gamma_j(0, \varepsilon_{\text{IR}}) &= \frac{\gamma_j}{\varepsilon_{\text{IR}}}, \quad \Gamma_j(m_j \neq 0, \varepsilon_{\text{IR}}) = \frac{C_F}{\varepsilon_{\text{IR}}}, \end{aligned} \quad (35)$$

where $C_F = 4/3$, $\gamma_q = 2$, and $\gamma_g = 11/2 - n_f/3$. And s_{jk} , Q_{jk}^2 , v_{jk} , and ρ_n are kinematic

variables defined as follows

$$\begin{aligned}
s_{jk} &= 2p_j p_k, & Q_{jk}^2 &= s_{jk} + m_j^2 + m_k^2, & v_{jk} &= \sqrt{1 - \frac{m_j^2 m_k^2}{(p_j p_k)^2}}, \\
\rho_n &= \sqrt{\frac{1 - v_{jk} + 2m_n^2/(Q_{jk}^2 - m_j^2 - m_k^2)}{1 + v_{jk} + 2m_n^2/(Q_{jk}^2 - m_j^2 - m_k^2)}} & (n = j, k).
\end{aligned} \tag{36}$$

When inserting Eq. (34) into the LO amplitudes for the $q\bar{q}$ and gg subprocesses as shown in Eq. (33), we can see that the IR divergences, including the $1/\epsilon_{\text{IR}}$ terms, can be written as combinations of the LO color correlated squared amplitudes and all the IR divergences from the virtual corrections in Eq. (26) are canceled exactly, as we expected.

IV. NUMERICAL RESULTS

In the Lagrangian \mathcal{L}_{NP} , there are totally nine free parameter $C_{\text{LL}}^1, C_{\text{LR}}^1, C_{\text{RL}}^1, C_{\text{RR}}^1, C_{\text{LL}}^8, C_{\text{LR}}^8, C_{\text{RL}}^8, C_{\text{RR}}^8$ and Λ . If we include left-handed top quark t_L in the \mathcal{L}_{NP} , it is suitable to work in $SU(2)_L$ doublet of the third-generation quarks $(t_L, b_L)^T$. However, the Wilson coefficients $C_{\text{LL}}^1, C_{\text{LL}}^8, C_{\text{RL}}^1$ and C_{RL}^8 are highly constrained by the LEP data for the ratio of $b\bar{b}$ to hadron production [82]:

$$B_b = 0.121629 \pm 0.00066, \tag{37}$$

which agrees well with the SM prediction. Thus, for simplicity we choose $C_{\text{LL}}^1 = C_{\text{LL}}^8 = C_{\text{RL}}^1 = C_{\text{RL}}^8 = 0$ [19]. Up to $\mathcal{O}(\alpha_s^2/\Lambda^2)$, contributions from color singlet operators due to mixing effects are much less than contributions from color octet operators, so we only consider color octet interactions. As a result, in the numerical calculations there are only three free NP parameters in the Lagrangian, i.e. $C_{\text{LR}}^8, C_{\text{RR}}^8$ and Λ .

Top quark mass is taken to be $m_t = 172.5$ GeV. We choose CTEQ6L and CTEQ6M PDF sets [83] and the associated α_s functions for LO and NLO calculation, respectively. Both the renormalization and factorization scales are fixed to the top quark mass unless specified. We have used the modified MadDipole [84] package for the real corrections.

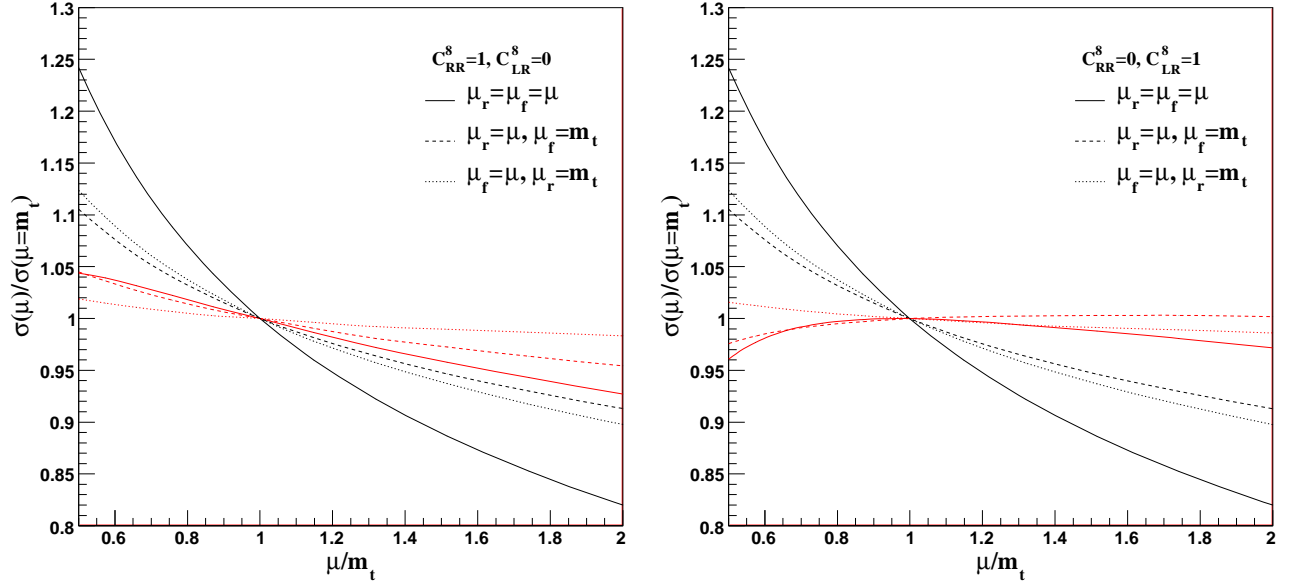


FIG. 6: Scale dependence of the total cross section at the Tevatron, the black and the red lines represent LO and NLO results, respectively.

A. Scale dependence

In Fig. 6 we show the scale dependence of the LO and NLO total cross section at the Tevatron for three cases: (1) the renormalization scale dependence $\mu_r = \mu$, $\mu_f = m_t$, (2) the factorization scale dependence $\mu_r = m_t$, $\mu_f = \mu$, and (3) total scale dependence $\mu_r = \mu_f = \mu$. It can be seen that the NLO corrections reduce the scale dependence significantly for all three cases, which makes the theoretical predictions more reliable.

B. Tevatron constraints

A_{FB} of top quark pair productions is defined as

$$\begin{aligned}
 A_{\text{FB}} &= \frac{\sigma_{\text{F}} - \sigma_{\text{B}}}{\sigma_{\text{F}} + \sigma_{\text{B}}} \\
 &= A_{\text{FB}}^{\text{NP}} \times R + A_{\text{FB}}^{\text{SM}} \times (1 - R)
 \end{aligned}$$

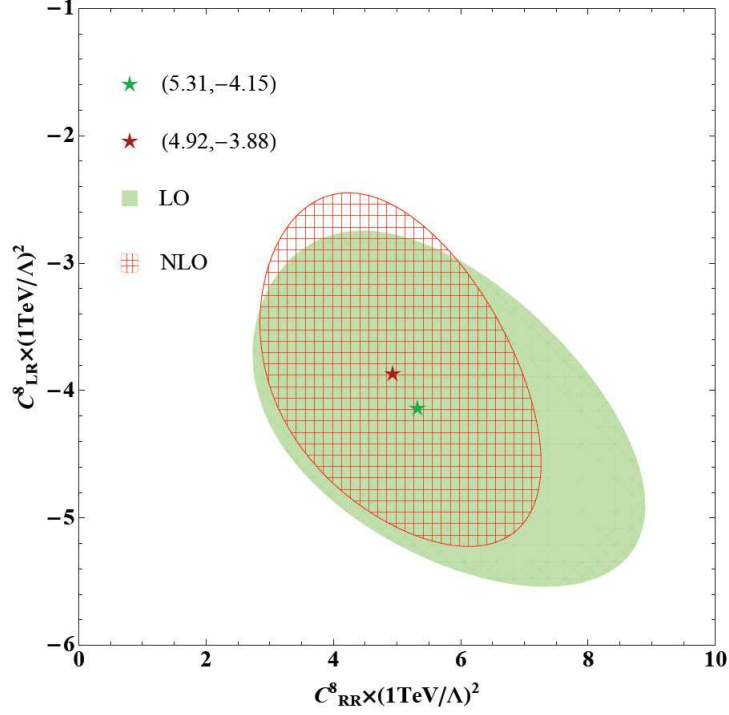


FIG. 7: Values of C_{RR}^8 and C_{LR}^8 allowed by the Tavetron data at 1σ CL: $\sigma_{t\bar{t}}=(7.50 \pm 0.48)\text{pb}$ and $A_{\text{FB}}(m_{t\bar{t}} > 450 \text{ GeV})=0.475\pm 0.114$. The green star $(5.31, -4.15)$ and red star $(4.92, -3.88)$ represent the BFPs at LO and NLO level, respectively.

where

$$\begin{aligned}
A_{\text{FB}}^{\text{NP}} &= (\sigma_{\text{F}}^{\text{NP}} - \sigma_{\text{B}}^{\text{NP}})/(\sigma_{\text{F}}^{\text{NP}} + \sigma_{\text{B}}^{\text{NP}}), \\
A_{\text{FB}}^{\text{SM}} &= (\sigma_{\text{F}}^{\text{SM}} - \sigma_{\text{B}}^{\text{SM}})/(\sigma_{\text{F}}^{\text{SM}} + \sigma_{\text{B}}^{\text{SM}}), \\
R &= \sigma_{\text{tot}}^{\text{NP}}/(\sigma_{\text{tot}}^{\text{SM}} + \sigma_{\text{tot}}^{\text{NP}})
\end{aligned} \tag{38}$$

are the asymmetries induced by NP and SM, and R is the fraction of NP contribution to the total cross section. σ_{F} and σ_{B} denote the total cross sections in the forward(F) and backward(B) rapidity regions, respectively. Up to order $O(\alpha_s^2/\Lambda^2)$, total cross sections induced by NP can be written as

$$\sigma_{\text{LO}}^{\text{NP}} = [(0.428_{-0.076}^{+0.103})C_{\text{RR}}^8 + (0.428_{-0.075}^{+0.101})C_{\text{LR}}^8] \left(\frac{1\text{TeV}}{\Lambda}\right)^2 \text{ pb}, \tag{39}$$

$$\sigma_{\text{NLO}}^{\text{NP}} = [(0.442_{-0.032}^{+0.018})C_{\text{RR}}^8 + (0.435_{-0.022}^{+0.022})C_{\text{LR}}^8] \left(\frac{1\text{TeV}}{\Lambda}\right)^2 \text{ pb}, \tag{40}$$

and the difference of the cross section in the forward and backward rapidity regions can be written as

$$[\sigma_{\text{F}}^{\text{NP}} - \sigma_{\text{B}}^{\text{NP}}]_{\text{LO}}^{m_{t\bar{t}} > 450 \text{ GeV}} = [(0.118_{-0.023}^{+0.031})C_{\text{RR}}^8 - (0.118_{-0.023}^{+0.031})C_{\text{LR}}^8] \left(\frac{1\text{TeV}}{\Lambda}\right)^2 \text{ pb}, \quad (41)$$

$$[\sigma_{\text{F}}^{\text{NP}} - \sigma_{\text{B}}^{\text{NP}}]_{\text{NLO}}^{m_{t\bar{t}} > 450 \text{ GeV}} = [(0.149_{-0.009}^{+0.003})C_{\text{RR}}^8 - (0.103_{-0.025}^{+0.008})C_{\text{LR}}^8] \left(\frac{1\text{TeV}}{\Lambda}\right)^2 \text{ pb}, \quad (42)$$

where the errors are obtained by varying the scale between $\mu_r = \mu_f = m_t/2$ and $\mu_r = \mu_f = 2m_t$. From the expressions Eqs.(39 – 42) we can see that NLO corrections reduce the dependence of $\sigma_{\text{F}}^{\text{NP}} - \sigma_{\text{B}}^{\text{NP}}$ and σ^{NP} on the renormalization and factorization scales significantly.

In Fig. 7, we show the allowed region in the $(C_{\text{RR}}^8, C_{\text{LR}}^8)$ plane that is consistent with the Tevatron data [9]:

$$\begin{aligned} \sigma_{t\bar{t}}^{\text{EX}} &= (7.50 \pm 0.48)\text{pb}, \\ A_{\text{FB}}^{\text{EX}} &= 0.475 \pm 0.114, \quad \text{for } m_{t\bar{t}} > 450 \text{ GeV}. \end{aligned} \quad (43)$$

We use Monte Carlo programm MCFM [85] to get the cross section of the gluon fusion channel $gg \rightarrow t\bar{t}$ at the NLO QCD level. As for the process of $q\bar{q} \rightarrow t\bar{t}$, we have checked our value with the results given by MCFM at QCD NLO level, which are well consistent in the range of Monte Carlo integration error. Combining the contributions of these two channels we have the total cross section of $t\bar{t}$ production

$$\sigma_{t\bar{t}}^{\text{SM}} = 7.00_{-0.76}^{+0.36} \text{ pb}, \quad (44)$$

where we have considered scale uncertainty in the calculations. For consistency we have used the SM predicted values of $A_{\text{FB}}(m_{t\bar{t}} \geq 450\text{GeV}) = 0.088$ at NLO QCD level, although next-to-next-to-leading logarithmic (NNLL) SM QCD results are available [6]. In Fig. 7, green and red regions correspond to NP LO and NLO results at 1σ confidence level(CL), where we have considered theoretical and experimental uncertainty in the total cross section and only consider experimental uncertainty in the A_{FB} calculation. It can be seen that NLO corrections obviously change the allowed region of C_{RR}^8 and C_{LR}^1 . The green star (5.31, -4.15) and red star (4.92, -3.88) represent the best-fit point(BFP) at LO and NLO level, respectively, from which we can see higher order corrections reduce the BFP by about

7%. The $t\bar{t}$ total cross sections induced by NP at the NLO BFP (4.92, -3.88) are

$$\begin{aligned}\sigma_{t\bar{t},\text{LO}}^{\text{NP}} &= 0.445 \text{ pb}, \\ \sigma_{t\bar{t},\text{NLO}}^{\text{NP}} &= 0.497 \text{ pb},\end{aligned}\tag{45}$$

where the K factor is about 1.12. A_{FB} containing NP contributions at the NLO BFP are shown together in Table I. The NLO QCD corrections to A_{FB} can reach about 10%, and the theoretical predictions containing NP NLO effects are consistent with experimental results at 2σ CL.

In Fig. 8, we show differential cross section $d\sigma/dm_{t\bar{t}}$ when we consider NP effects at

	SM NLO QCD + NP LO	SM NLO QCD + NP NLO
$A_{\text{FB}}^{p\bar{p}}$	0.175	0.189 ($\sim 0.7 \sigma$)
$A_{\text{FB}}^{t\bar{t}}$	0.252	0.275 ($\sim 1.6 \sigma$)
$A_{\text{FB}}^{t\bar{t}} (m_{t\bar{t}} < 450 \text{ GeV})$	0.132	0.136 ($\sim 1.6 \sigma$)
$A_{\text{FB}}^{t\bar{t}} (m_{t\bar{t}} > 450 \text{ GeV})$	0.452	0.475 ($\sim 0 \sigma$)
$A_{\text{FB}}^{t\bar{t}} (\Delta y < 1)$	0.170	0.161 ($\sim 0.9 \sigma$)
$A_{\text{FB}}^{t\bar{t}} (\Delta y > 1)$	0.719	0.681 ($\sim 0.3 \sigma$)

TABLE I: A_{FB} with $C_{\text{RR}}^8(1\text{TeV}/\Lambda)^2 = 4.92$ and $C_{\text{LR}}^8(1\text{TeV}/\Lambda)^2 = -3.88$ at the Tevtron, where $A_{\text{FB}}^{p\bar{p}}$ and $A_{\text{FB}}^{t\bar{t}}$ are the A_{FB} in the lab frame and the $t\bar{t}$ rest frame, respectively, and $\Delta y = y_t - y_{\bar{t}}$ is the difference of rapidities of the top and antitop quarks. Here we list the CL when containing NP effects at NLO level.

the NLO BFP, from which we can see that higher order corrections do not change the distribution very much.

C. LHC predictions

The process of top quark pair production has been measured at the LHC, and the cross section [87, 88] is

$$\begin{aligned}\sigma_{t\bar{t}}^{\text{ATLAS}}(\sqrt{S} = 7 \text{ TeV}) &= 180 \pm 18\text{pb}, \\ \sigma_{t\bar{t}}^{\text{CMS}}(\sqrt{S} = 7 \text{ TeV}) &= 158 \pm 19\text{pb},\end{aligned}\tag{46}$$

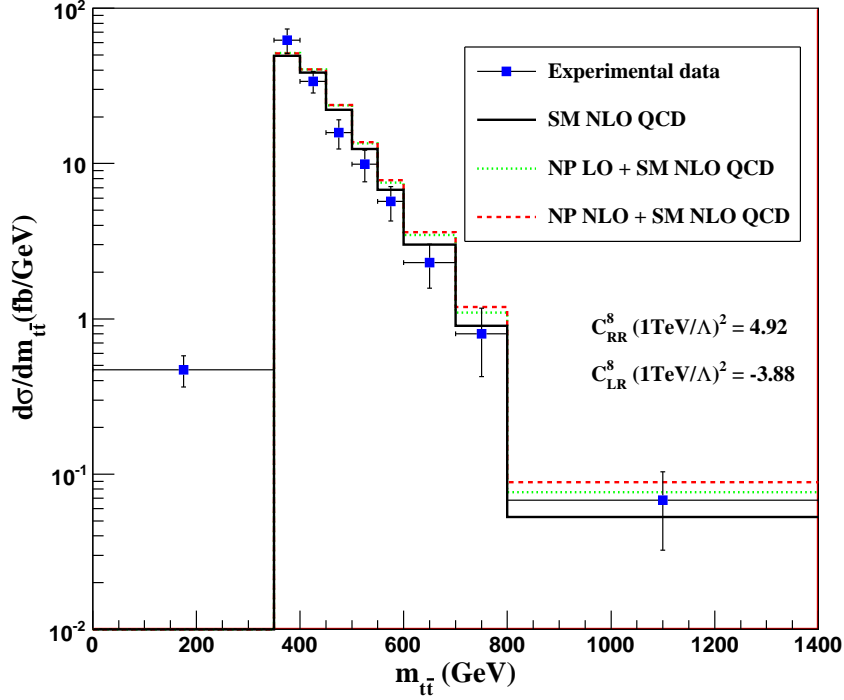


FIG. 8: Differential cross sections $d\sigma/dm_{t\bar{t}}$ as a function of $m_{t\bar{t}}$ at the NLO BFP (4.92, -3.88). Here "Experimental data" is $d\sigma/dm_{t\bar{t}}$ measured with 2.7 fb^{-1} of integrated luminosity at the Tevatron [86]. "SM NLO QCD" represents the results in the SM QCD at NLO level. "NP LO + SM NLO QCD" and "NP NLO + SM NLO QCD" stand for the predictions including NP effects up to $\mathcal{O}(\alpha_s/\Lambda^2)$ and $\mathcal{O}(\alpha_s^2/\Lambda^2)$, respectively.

which is consistent with the SM predictions. The NP contributions at the NLO BFP (4.92, -3.88) is about 3 pb, which is much smaller than the experimental uncertainty. Thus, it is difficult to measure the NP effects only through the cross section measurements. In Fig. 9, we show differential cross section $d\sigma/dm_{t\bar{t}}$ at the LHC when we consider NP effects at the NLO BFP (4.92, -3.88), from which we can see that NP contributions almost do not change the distribution.

Since the LHC is a proton-proton collider, which is forward-backward symmetric, the A_{FB} defined at Tevatron can not be directly applied to the proton-proton collider experiments at the LHC. The A_{C} used by CMS [89] can be written as

$$A_{\text{C}} = \frac{\sigma(|\eta_t| - |\eta_{\bar{t}}| > 0) - \sigma(|\eta_t| - |\eta_{\bar{t}}| < 0)}{\sigma(|\eta_t| - |\eta_{\bar{t}}| > 0) + \sigma(|\eta_t| - |\eta_{\bar{t}}| < 0)}, \quad (47)$$

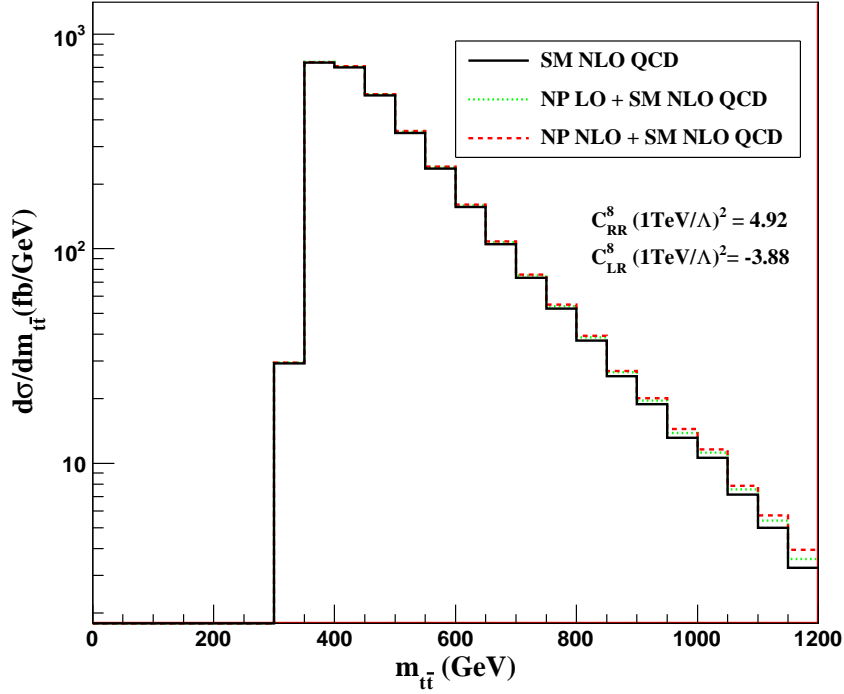


FIG. 9: Differential cross sections $d\sigma/dm_{t\bar{t}}$ as a function of $m_{t\bar{t}}$ at the LHC with $\sqrt{S} = 7$ TeV.

where η_t and $\eta_{\bar{t}}$ are pseudo rapidities of top and antitop quark, respectively. Its value is measured to be

$$A_C = -0.016 \pm 0.030(\text{stat.})_{-0.019}^{+0.010}(\text{syst.}) \quad (48)$$

which is consistent with the SM predictions: $A_C = 0.013(11)$ [17, 89, 90]. The A_C induced by NP interactions at the NP NLO BFP (4.92, -3.88) is 0.063, which is about 5 times larger than SM predictions, and also consistent with the CMS data at about 2σ CL.

In Fig. 10, we show the results of a combined fit to the $t\bar{t}$ data in the presence of NP at different CLs. The blue contours from dark to light indicate the experimentally preferred region of 68%, 95% and 99% CL in the (C_{RR}^8, C_{LR}^8) plane. The black dot represent the SM point (0, 0), and the black star represent the NP NLO BFP (4.92, -3.88). The black dotted and dashed lines respectively represent the value of $t\bar{t}$ cross section and the A_C at the LHC with $\sqrt{S} = 7$ TeV. From the location of the blue area, one finds that A_C predicted by NP is obviously much larger than SM predictions, and LHC has potential to find this difference when the measurement precision increases.

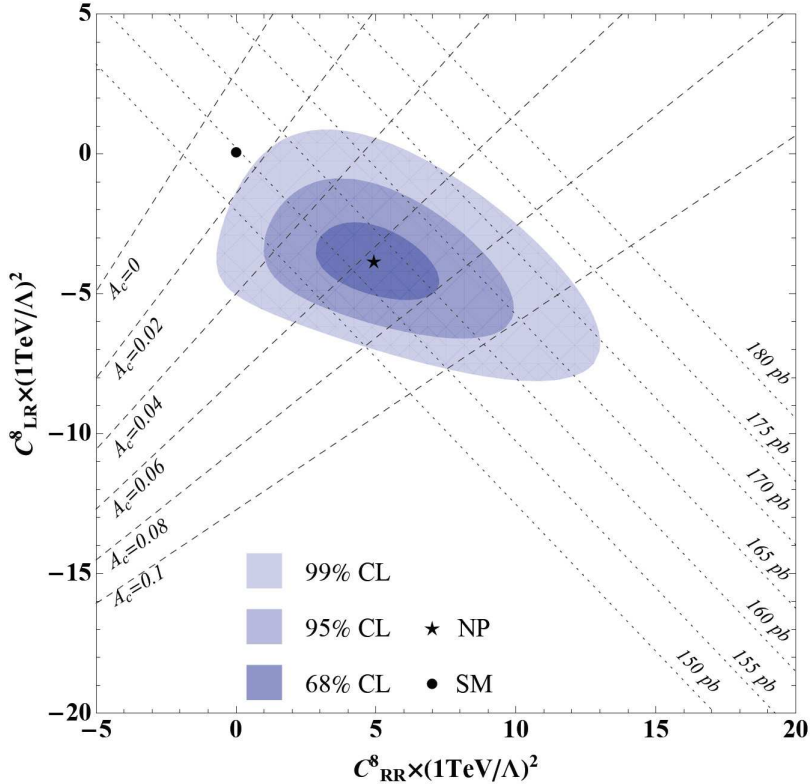


FIG. 10: Results of a combined fit to $\sigma_{t\bar{t}}$ and the value of A_{FB} allowing for NP at different CLs. The blue contours from dark to light indicate the experimentally favored region of 68%, 95% and 99% CL in the (C_{RR}^8, C_{LR}^8) plane. The black dotted and dashed lines respectively represent the value of $t\bar{t}$ cross section and the A_C at the LHC with $\sqrt{S} = 7$ TeV. The black dot and black star represent the SM point and the NP NLO BFP.

V. CONCLUSIONS

In conclusion, we have investigated A_{FB} and total cross section of top quark pair production induced by dimension-six four quark operators at the Tevatron up to $\mathcal{O}(\alpha_s^2/\Lambda^2)$. Our results show that, NLO QCD corrections can change A_{FB} and the total cross section by about 10%. Moreover, NLO QCD corrections reduce the dependence of A_{FB} and the total cross sections on the renormalization and factorization scales significantly, which lead to increased confidence on the theoretical predictions. We also evaluate total cross section and A_C induced by these operators at the LHC up to $\mathcal{O}(\alpha_s^2/\Lambda^2)$, for the parameter space allowed by the Tevatron data. We find that the value of A_C induced by these operators is

much larger than SM predictions, and LHC has potential to discover these NP effects when the measurement precision increases.

Acknowledgments

We would like to thank Rikkert Frederix, Kouhei Hasegawa and Sven-Olaf Moch for helpful discussion. This work was supported in part by the National Natural Science Foundation of China, under Grants No. 11021092 and No. 10975004.

Appendix A: FINITE TERMS IN VIRTUAL CORRECTIONS

In this appendix, we collect explicit expressions of finite terms in virtual corrections. Analytical continuation for the Mandelstam variables are defined as

$$\begin{aligned}
 s &\rightarrow s + i\varepsilon, \\
 u &\rightarrow u + i\varepsilon, \\
 t &\rightarrow t + i\varepsilon.
 \end{aligned}
 \tag{A1}$$

For simplicity, we introduce the following abbreviations.

$$c_t = \frac{m_t^2 - t}{t}, \quad c_u = \frac{m_t^2 - u}{u},
 \tag{A2}$$

$$\begin{aligned}
 y_1(t) &= \ln \frac{t_1}{\mu_r^2} + \frac{t_1}{2t} - 1, \\
 y_2(t) &= \ln \frac{m_t^2}{\mu_r^2} + \frac{t_1}{t} - 1, \\
 y_3(t) &= \ln \frac{t_1}{\mu_r^2} - \left(\frac{t_1}{t} + 1 \right), \\
 y_4(t) &= \ln \frac{m_t^2}{\mu_r^2} - 2 \left(\frac{t_1}{t} + 2 \right),
 \end{aligned}
 \tag{A3}$$

$$\begin{aligned}
f_1(t) &= \frac{3}{8t} \left(\frac{2}{c_t^2} + \frac{2}{c_t} + \ln \frac{t_1}{m_t^2} \right), \\
f_2(t) &= \frac{3}{4} \left(1 + \frac{1}{c_t} \right) \left(1 - c_t \ln \frac{t_1}{m_t^2} \right), \\
f_3(t) &= -\frac{1}{2} y_1^2(t) + \frac{1}{4} y_2^2(t) - \frac{1}{8} c_t^2 - \frac{1}{2c_t} - \frac{\pi^2}{12} - \frac{5}{4} + \text{Li}_2 \left(\frac{-t}{t_1} \right), \\
f_4(t) &= -\frac{1}{2} y_3^2(t) + \frac{1}{4} y_4^2(t) - \frac{1}{2} c_t^2 - 3c_t - \frac{1}{c_t} - \frac{\pi^2}{12} - \frac{3}{2} + \text{Li}_2 \left(\frac{-t}{t_1} \right), \\
f_5(t, u) &= \frac{3}{2} f_3(t) - \frac{3}{2} f_4(u), \tag{A4}
\end{aligned}$$

$$\begin{aligned}
h_1(s) &= \frac{1}{32} \left(\beta + \frac{1}{\beta} \right) \ln \left(\frac{\beta + 1}{\beta - 1} \right) \left(2\ln\beta - 3 + \ln \frac{m_t^2}{\mu_r^2} + \ln \left(\frac{-s}{\mu_r^2} \right) \right), \\
h_2(s) &= \frac{1}{16} \left(\beta + \frac{1}{\beta} \right) \left(\text{Li}_2 \left(\frac{\beta - 1}{2\beta} \right) - \text{Li}_2 \left(\frac{\beta + 1}{2\beta} \right) \right), \\
h_3(s) &= -\frac{\beta^3}{16} \ln \left(\frac{\beta + 1}{\beta - 1} \right) + \frac{\beta^2}{8} + \frac{3\beta}{16} \ln \left(\frac{\beta + 1}{\beta - 1} \right) + \frac{1}{16} \ln^2 \left(\frac{-s}{\mu_r^2} \right), \\
&\quad -\frac{21}{16} \ln \frac{m_t^2}{\mu_r^2} - \frac{3 - 2n_f}{16} \ln \left(\frac{-s}{\mu_r^2} \right) - \frac{5n_f - 61}{24}, \\
h_4(s) &= -\frac{\beta^3}{16} \ln \left(\frac{\beta + 1}{\beta - 1} \right) + \frac{\beta^2}{8} + \frac{5\beta}{32} \ln \left(\frac{\beta + 1}{\beta - 1} \right) + \frac{1}{8} \ln \frac{m_t^2}{\mu_r^2}, \\
&\quad -\frac{1}{3} + \frac{1}{32\beta} \ln \left(\frac{\beta + 1}{\beta - 1} \right), \\
h_5(s) &= \frac{1}{16s\beta} \ln \left(\frac{\beta + 1}{\beta - 1} \right), \\
h_6(s) &= n_f \left(\frac{1}{8} \ln \left(\frac{-s}{\mu_r^2} \right) - \frac{5}{24} \right), \\
h_7(s) &= -\frac{1}{2} \ln^2 \left(\frac{-s}{\mu_r^2} \right) + \frac{3}{2} \ln \left(\frac{-s}{\mu_r^2} \right) - 2 \ln \frac{m_t^2}{\mu_r^2} - \frac{1}{2}, \\
h_8(s) &= \frac{1}{4} \left(\beta - \frac{1}{\beta} \right) \ln \left(\frac{\beta + 1}{\beta - 1} \right), \\
h_9(s) &= -8h_1(s) - 8h_2(s) + h_7(s), \tag{A5}
\end{aligned}$$

$$\begin{aligned}
g_1(s, f_3(t), f_4(u)) &= \frac{7}{4} f_3(t) + \frac{1}{2} f_4(u) + h_1(s) + h_2(s) + h_3(s), \\
g_2(s, t) &= \frac{7}{6} f_2(t) + h_4(s), \\
g_3(s, u) &= \frac{1}{3} f_2(u) + h_4(s), \\
g_4(s, t) &= -\frac{7}{6} f_1(t) - h_5(s), \\
g_5(s, u) &= -\frac{1}{3} f_1(u) - h_5(s). \tag{A6}
\end{aligned}$$

First we list the amplitude for helicity (+ - ++),

$$i\mathcal{M}_{\text{virt}}^{\text{NP,fin}}(+ - ++) = \frac{i\alpha_s m}{\pi\Lambda^2} C_F [\mathcal{M}_{\text{ss}}(+ - ++) \mathcal{C}_1 + \mathcal{M}_{\text{so}}(+ - ++) \mathcal{C}_8 + \mathcal{M}_{\text{os}}(+ - ++) \mathcal{C}_1 + \mathcal{M}_{\text{oo}}(+ - ++) \mathcal{C}_8], \quad (\text{A7})$$

where

$$\begin{aligned} \mathcal{M}_{\text{ss}}(+ - ++) &= C_{\text{RL}}^1 [h_8(s)\mathcal{M}_1 + h_9(s)\mathcal{M}_2 + 8h_5(s) (\mathcal{M}_1^{(m)} + \mathcal{M}_2^{(m)})] \\ &\quad + C_{\text{RR}}^1 [h_9(s)\mathcal{M}_1 + h_8(s)\mathcal{M}_2 + 8h_5(s) (\mathcal{M}_1^{(m)} + \mathcal{M}_2^{(m)})], \end{aligned} \quad (\text{A8})$$

$$\begin{aligned} \mathcal{M}_{\text{so}}(+ - ++) &= -C_{\text{RL}}^1 [f_2(u)\mathcal{M}_1 + f_5(u, t)\mathcal{M}_2 - f_1(u) (\mathcal{M}_1^{(m)} + \mathcal{M}_2^{(m)})] \\ &\quad + C_{\text{RR}}^1 [f_5(t, u)\mathcal{M}_1 + f_2(t)\mathcal{M}_2 - f_1(t) (\mathcal{M}_1^{(m)} + \mathcal{M}_2^{(m)})], \end{aligned} \quad (\text{A9})$$

$$\begin{aligned} \mathcal{M}_{\text{os}}(+ - ++) &= -\frac{2}{9} C_{\text{RL}}^8 [f_2(u)\mathcal{M}_1 + f_5(u, t)\mathcal{M}_2 - f_1(u) (\mathcal{M}_1^{(m)} + \mathcal{M}_2^{(m)})] \\ &\quad + \frac{2}{9} C_{\text{RR}}^8 [f_5(t)\mathcal{M}_1 + f_2(t)\mathcal{M}_2 - f_1(t) (\mathcal{M}_1^{(m)} + \mathcal{M}_2^{(m)})], \end{aligned} \quad (\text{A10})$$

$$\begin{aligned} \mathcal{M}_{\text{oo}}(+ - ++) &= C_{\text{RL}}^8 [g_3(s, u)\mathcal{M}_1 + g_1(s, f_4(t), f_3(u)) \mathcal{M}_2 + g_5(s, u) (\mathcal{M}_1^{(m)} + \mathcal{M}_2^{(m)})] \\ &\quad + C_{\text{RR}}^8 [g_1(s, f_3(t), f_4(u)) \mathcal{M}_1 + g_2(s, t)\mathcal{M}_2 + g_4(s, t) (\mathcal{M}_1^{(m)} + \mathcal{M}_2^{(m)})] \\ &\quad + C_{\text{LR}}^8 h_6(s)\mathcal{M}_1 + C_{\text{LL}}^8 h_6(s)\mathcal{M}_2. \end{aligned} \quad (\text{A11})$$

Similarly, amplitude for helicity (- + ++) can be written as

$$i\mathcal{M}_{\text{virt}}^{\text{NP,fin}}(- + ++) = \frac{i\alpha_s m}{\pi\Lambda^2} C_F [\mathcal{M}_{\text{ss}}(- + ++) \mathcal{C}_1 + \mathcal{M}_{\text{so}}(- + ++) \mathcal{C}_8 + \mathcal{M}_{\text{os}}(- + ++) \mathcal{C}_1 + \mathcal{M}_{\text{oo}}(- + ++) \mathcal{C}_8], \quad (\text{A12})$$

where

$$\begin{aligned} \mathcal{M}_{\text{ss}}(- + ++) &= C_{\text{LR}}^1 [h_9(s)\mathcal{M}_3 + h_8(s)\mathcal{M}_4 - 8h_5(s) (\mathcal{M}_3^{(m)} + \mathcal{M}_4^{(m)})] \\ &\quad + C_{\text{LL}}^1 [h_8(s)\mathcal{M}_3 + h_9(s)\mathcal{M}_4 - 8h_5(s) (\mathcal{M}_3^{(m)} + \mathcal{M}_4^{(m)})], \end{aligned} \quad (\text{A13})$$

$$\begin{aligned} \mathcal{M}_{\text{so}}(- + ++) &= -C_{\text{LR}}^1 [f_5(u, t)\mathcal{M}_3 + f_2(u)\mathcal{M}_4 + f_1(u) (\mathcal{M}_3^{(m)} + \mathcal{M}_4^{(m)})] \\ &\quad + C_{\text{LL}}^1 [f_2(t)\mathcal{M}_3 + f_5(t, u)\mathcal{M}_4 + f_1(t) (\mathcal{M}_3^{(m)} + \mathcal{M}_4^{(m)})], \end{aligned} \quad (\text{A14})$$

$$\begin{aligned} \mathcal{M}_{\text{os}}(- + ++) &= -\frac{2}{9} C_{\text{LR}}^8 [f_5(u, t)\mathcal{M}_3 + f_2(u)\mathcal{M}_4 + f_1(u) (\mathcal{M}_3^{(m)} + \mathcal{M}_4^{(m)})] \\ &\quad + \frac{2}{9} C_{\text{LL}}^8 [f_2(t)\mathcal{M}_3 + f_5(t, u)\mathcal{M}_4 + f_1(t) (\mathcal{M}_3^{(m)} + \mathcal{M}_4^{(m)})], \end{aligned} \quad (\text{A15})$$

$$\begin{aligned} \mathcal{M}_{\text{oo}}(- + ++) &= C_{\text{LL}}^8 [g_2(s, t)\mathcal{M}_3 + g_1(s, f_3(t), f_4(u)) \mathcal{M}_4 - g_4(s, t) (\mathcal{M}_3^{(m)} + \mathcal{M}_4^{(m)})] \\ &\quad + C_{\text{LR}}^8 [g_1(s, f_4(t), f_3(u)) \mathcal{M}_3 + g_3(s, u)\mathcal{M}_4 - g_5(s, u) (\mathcal{M}_3^{(m)} + \mathcal{M}_4^{(m)})] \\ &\quad + C_{\text{RL}}^8 h_6(s)\mathcal{M}_4 + C_{\text{RR}}^8 h_6(s)\mathcal{M}_3. \end{aligned} \quad (\text{A16})$$

Appendix B: evolution equation of Wilson coefficients

In this appendix we present the evaluation equations of the Wilson coefficients C_{AB}^1 and C_{AB}^8 , expanded to $\mathcal{O}(\alpha_s)$.

$$C_{LL}^1(\mu_r) = C_{LL}^1(m_t) - 0.0397887C_F\alpha_s \ln \frac{m_t}{\mu_r} C_{LL}^8(m_t), \quad (\text{B1})$$

$$\begin{aligned} C_{LL}^8(\mu_r) &= C_{LL}^8(m_t) - 0.0497359C_F\alpha_s \ln \frac{m_t}{\mu_r} C_{RL}^8(m_t) \\ &\quad - 0.179049C_F\alpha_s \ln \frac{m_t}{\mu_r} C_{LL}^1(m_t) \\ &\quad - 0.00994718C_F\alpha_s \ln \frac{m_t}{\mu_r} C_{LR}^8(m_t), \end{aligned} \quad (\text{B2})$$

$$C_{LR}^1(\mu_r) = C_{LR}^1(m_t) + 0.0397887C_F\alpha_s \ln \frac{m_t}{\mu_r} C_{LR}^8(m_t), \quad (\text{B3})$$

$$\begin{aligned} C_{LR}^8(\mu_r) &= C_{LR}^8(m_t) + 0.149208C_F\alpha_s \ln \frac{m_t}{\mu_r} C_{LR}^8(m_t) \\ &\quad - 0.0497359C_F\alpha_s \ln \frac{m_t}{\mu_r} C_{RR}^8(m_t) \\ &\quad - 0.00994718C_F\alpha_s \ln \frac{m_t}{\mu_r} C_{LL}^8(m_t) \\ &\quad + 0.179049C_F\alpha_s \ln \frac{m_t}{\mu_r} C_{LR}^1(m_t), \end{aligned} \quad (\text{B4})$$

$$C_{RL}^1(\mu_r) = C_{RL}^1(m_t) + 0.0397887C_F\alpha_s \ln \frac{m_t}{\mu_r} C_{RL}^8(m_t), \quad (\text{B5})$$

$$\begin{aligned} C_{RL}^8(\mu_r) &= C_{RL}^8(m_t) + 0.149208C_F\alpha_s \ln \frac{m_t}{\mu_r} C_{RL}^8(m_t) \\ &\quad - 0.0497359C_F\alpha_s \ln \frac{m_t}{\mu_r} C_{LL}^8(m_t) \\ &\quad - 0.00994718C_F\alpha_s \ln \frac{m_t}{\mu_r} C_{RR}^8(m_t) \\ &\quad + 0.179049C_F\alpha_s \ln \frac{m_t}{\mu_r} C_{RL}^1(m_t), \end{aligned}$$

$$C_{RR}^1(\mu_r) = C_{RR}^1(m_t) - 0.0397887C_F\alpha_s \ln \frac{m_t}{\mu_r} C_{RR}^8(m_t), \quad (\text{B6})$$

$$\begin{aligned} C_{RR}^8(\mu_r) &= C_{RR}^8(m_t) - 0.0497359C_F\alpha_s \ln \frac{m_t}{\mu_r} C_{LR}^8(m_t) \\ &\quad - 0.00994718C_F\alpha_s \ln \frac{m_t}{\mu_r} C_{RL}^8(m_t) \\ &\quad - 0.179049C_F\alpha_s \ln \frac{m_t}{\mu_r} C_{RR}^1(m_t). \end{aligned} \quad (\text{B7})$$

[1] J. H. Kuhn and G. Rodrigo, Phys. Rev. Lett. **81**, 49 (1998), hep-ph/9802268.

[2] J. H. Kuhn and G. Rodrigo, Phys. Rev. **D59**, 054017 (1999), hep-ph/9807420.

- [3] M. T. Bowen, S. D. Ellis, and D. Rainwater, Phys. Rev. **D73**, 014008 (2006), hep-ph/0509267.
- [4] L. G. Almeida, G. F. Sterman, and W. Vogelsang, Phys. Rev. **D78**, 014008 (2008), 0805.1885.
- [5] O. Antunano, J. H. Kuhn, and G. Rodrigo, Phys. Rev. **D77**, 014003 (2008), 0709.1652.
- [6] V. Ahrens, A. Ferroglia, M. Neubert, B. D. Pecjak, and L. L. Yang (2011), 1106.6051.
- [7] V. M. Abazov et al. (D0), Phys. Rev. Lett. **100**, 142002 (2008), 0712.0851.
- [8] T. Aaltonen et al. (CDF), Phys. Rev. Lett. **101**, 202001 (2008), 0806.2472.
- [9] T. Aaltonen et al. (CDF), Phys. Rev. **D83**, 112003 (2011), 1101.0034.
- [10] Y.-C. C. f. t. C. collaboration (2011), 1107.0239.
- [11] A. Djouadi, G. Moreau, F. Richard, and R. K. Singh, Phys. Rev. **D82**, 071702 (2010), 0906.0604.
- [12] S. Jung, H. Murayama, A. Pierce, and J. D. Wells, Phys. Rev. **D81**, 015004 (2010), 0907.4112.
- [13] K. Cheung, W.-Y. Keung, and T.-C. Yuan, Phys. Lett. **B682**, 287 (2009), 0908.2589.
- [14] P. H. Frampton, J. Shu, and K. Wang, Phys. Lett. **B683**, 294 (2010), 0911.2955.
- [15] J. Shu, T. M. P. Tait, and K. Wang, Phys. Rev. **D81**, 034012 (2010), 0911.3237.
- [16] A. Arhrib, R. Benbrik, and C.-H. Chen, Phys. Rev. **D82**, 034034 (2010), 0911.4875.
- [17] P. Ferrario and G. Rodrigo, JHEP **02**, 051 (2010), 0912.0687.
- [18] I. Dorsner, S. Fajfer, J. F. Kamenik, and N. Kosnik, Phys. Rev. **D81**, 055009 (2010), 0912.0972.
- [19] D.-W. Jung, P. Ko, J. S. Lee, and S.-h. Nam, Phys. Lett. **B691**, 238 (2010), 0912.1105.
- [20] J. Cao, Z. Heng, L. Wu, and J. M. Yang, Phys. Rev. **D81**, 014016 (2010), 0912.1447.
- [21] V. Barger, W.-Y. Keung, and C.-T. Yu, Phys. Rev. **D81**, 113009 (2010), 1002.1048.
- [22] Q.-H. Cao, D. McKeen, J. L. Rosner, G. Shaughnessy, and C. E. M. Wagner, Phys. Rev. **D81**, 114004 (2010), 1003.3461.
- [23] B. Xiao, Y.-k. Wang, and S.-h. Zhu, Phys. Rev. **D82**, 034026 (2010), 1006.2510.
- [24] M. V. Martynov and A. D. Smirnov, Mod. Phys. Lett. **A25**, 2637 (2010), 1006.4246.
- [25] R. S. Chivukula, E. H. Simmons, and C. P. Yuan, Phys. Rev. **D82**, 094009 (2010), 1007.0260.
- [26] M. Bauer, F. Goertz, U. Haisch, T. Pfoh, and S. Westhoff, JHEP **11**, 039 (2010), 1008.0742.
- [27] C.-H. Chen, G. Cvetič, and C. S. Kim, Phys. Lett. **B694**, 393 (2011), 1009.4165.
- [28] C. Degrande, J.-M. Gerard, C. Grojean, F. Maltoni, and G. Servant, JHEP **03**, 125 (2011), 1010.6304.
- [29] D.-W. Jung, P. Ko, and J. S. Lee, Phys. Lett. **B701**, 248 (2011), 1011.5976.

- [30] G. Burdman, L. de Lima, and R. D. Matheus, Phys. Rev. **D83**, 035012 (2011), 1011.6380.
- [31] D.-w. Jung, P. Ko, J. S. Lee, and S.-h. Nam (2010), 1012.0102.
- [32] D. Choudhury, R. M. Godbole, S. D. Rindani, and P. Saha (2010), 1012.4750.
- [33] K. Cheung and T.-C. Yuan, Phys. Rev. **D83**, 074006 (2011), 1101.1445.
- [34] J. Cao, L. Wang, L. Wu, and J. M. Yang (2011), 1101.4456.
- [35] E. L. Berger, Q.-H. Cao, C.-R. Chen, C. S. Li, and H. Zhang, Phys. Rev. Lett. **106**, 201801 (2011), 1101.5625.
- [36] V. Barger, W.-Y. Keung, and C.-T. Yu, Phys. Lett. **B698**, 243 (2011), 1102.0279.
- [37] B. Bhattacharjee, S. S. Biswal, and D. Ghosh, Phys. Rev. **D83**, 091501 (2011), 1102.0545.
- [38] K. Blum et al. (2011), 1102.3133.
- [39] K. M. Patel and P. Sharma, JHEP **04**, 085 (2011), 1102.4736.
- [40] G. Isidori and J. F. Kamenik, Phys. Lett. **B700**, 145 (2011), 1103.0016.
- [41] A. R. Zerwekh (2011), 1103.0956.
- [42] E. R. Barreto, Y. A. Coutinho, and J. Sa Borges, Phys. Rev. **D83**, 054006 (2011), 1103.1266.
- [43] R. Foot, Phys. Rev. **D83**, 114013 (2011), 1103.1940.
- [44] Z. Ligeti, G. M. Tavares, and M. Schmaltz, JHEP **06**, 109 (2011), 1103.2757.
- [45] J. A. Aguilar-Saavedra and M. Perez-Victoria, JHEP **05**, 034 (2011), 1103.2765.
- [46] M. I. Gresham, I.-W. Kim, and K. M. Zurek, Phys. Rev. **D83**, 114027 (2011), 1103.3501.
- [47] S. Jung, A. Pierce, and J. D. Wells, Phys. Rev. **D83**, 114039 (2011), 1103.4835.
- [48] M. R. Buckley, D. Hooper, J. Kopp, and E. T. Neil, Phys. Rev. **D83**, 115013 (2011), 1103.6035.
- [49] J. Shu, K. Wang, and G. Zhu (2011), 1104.0083.
- [50] J. A. Aguilar-Saavedra and M. Perez-Victoria, Phys. Lett. **B701**, 93 (2011), 1104.1385.
- [51] C.-H. Chen, S. S. C. Law, and R.-H. Li (2011), 1104.1497.
- [52] C. Degrande, J.-M. Gerard, C. Grojean, F. Maltoni, and G. Servant (2011), 1104.1798.
- [53] S. Jung, A. Pierce, and J. D. Wells (2011), 1104.3139.
- [54] D.-W. Jung, P. Ko, and J. S. Lee (2011), 1104.4443.
- [55] K. S. Babu, M. Frank, and S. K. Rai, Phys. Rev. Lett. **107**, 061802 (2011), 1104.4782.
- [56] A. Djouadi, G. Moreau, and F. Richard (2011), 1105.3158.
- [57] R. Barcelo, A. Carmona, M. Masip, and J. Santiago, Phys. Rev. **D84**, 014024 (2011), 1105.3333.
- [58] D. Krohn, T. Liu, J. Shelton, and L.-T. Wang (2011), 1105.3743.

- [59] J. A. Aguilar-Saavedra and M. Perez-Victoria (2011), 1105.4606.
- [60] A. Hektor et al. (2011), 1105.5644.
- [61] Y. Cui, Z. Han, and M. D. Schwartz (2011), 1106.3086.
- [62] R. Barcelo, A. Carmona, M. Masip, and J. Santiago (2011), 1106.4054.
- [63] E. Gabrielli and M. Raidal (2011), 1106.4553.
- [64] M. Duraisamy, A. Rashed, and A. Datta (2011), 1106.5982.
- [65] J. A. Aguilar-Saavedra and M. Perez-Victoria (2011), 1107.0841.
- [66] G. M. Tavares and M. Schmaltz (2011), 1107.0978.
- [67] L. Vecchi (2011), 1107.2933.
- [68] K. Blum, Y. Hochberg, and Y. Nir (2011), 1107.4350.
- [69] E. J. Eichten, K. D. Lane, and M. E. Peskin, Phys. Rev. Lett. **50**, 811 (1983).
- [70] E. Eichten, I. Hinchliffe, K. D. Lane, and C. Quigg, Rev. Mod. Phys. **56**, 579 (1984).
- [71] P. Chiappetta and M. Perrottet, Phys. Lett. **B253**, 489 (1991).
- [72] E. Eichten and K. D. Lane (1996), hep-ph/9609297.
- [73] J. Gao, C. S. Li, J. Wang, H. X. Zhu, and C. P. Yuan, Phys. Rev. Lett. **106**, 142001 (2011), 1101.4611.
- [74] J. F. Kamenik, J. Shu, and J. Zupan (2011), 1107.5257.
- [75] D.-W. Jung, P. Ko, J. S. Lee, and S.-H. Nam, PoS **ICHEP2010**, 397 (2010).
- [76] H. X. Zhu et al. (2011), 1106.2243.
- [77] Z. Bern, A. De Freitas, L. J. Dixon, and H. L. Wong, Phys. Rev. **D66**, 085002 (2002), hep-ph/0202271.
- [78] R. Kleiss and W. J. Stirling, Nucl. Phys. **B262**, 235 (1985).
- [79] S. Badger, J. M. Campbell, and R. K. Ellis, JHEP **03**, 027 (2011), 1011.6647.
- [80] S. Catani, S. Dittmaier, M. H. Seymour, and Z. Trocsanyi, Nucl. Phys. **B627**, 189 (2002), hep-ph/0201036.
- [81] J. G. Korner and Z. Merebashvili, Phys. Rev. **D66**, 054023 (2002), hep-ph/0207054.
- [82] K. Nakamura et al. (Particle Data Group), J. Phys. **G37**, 075021 (2010).
- [83] J. Pumplin et al., JHEP **07**, 012 (2002), hep-ph/0201195.
- [84] R. Frederix, T. Gehrmann, and N. Greiner, JHEP **09**, 122 (2008), 0808.2128.
- [85] J. M. Campbell and R. K. Ellis, Phys. Rev. **D60**, 113006 (1999), hep-ph/9905386.
- [86] T. Aaltonen et al. (CDF), Phys. Rev. Lett. **102**, 222003 (2009), 0903.2850.

- [87] M. Cristinziani (ATLAS) (2011), 1105.6302.
- [88] S. Tosi and o. b. o. t. C. Collaboration (2011), 1106.6158.
- [89] The CMS Collaboration (2011), CMS-PAS-TOP-10-014.
- [90] P. Ferrario and G. Rodrigo, Phys. Rev. **D78**, 094018 (2008), 0809.3354.